

Cascaded control concept of a robot with two degrees of freedom driven by four artificial pneumatic muscle actuators

A. Hildebrandt, O. Sawodny
Institute of Automation and Systems Engineering
Technische Universität Ilmenau
D-98684 Ilmenau, Germany

R. Neumann, A. Hartmann
Festo AG & Co.
Research Mechatronics
D-73734 Esslingen, Germany

Abstract—Pneumatic muscles are interesting in their use as actuators in robotics, since they have a high power/weight ratio, a high-tension force and a long durability. This paper presents a two-axis planar articulated robot, which is driven by four pneumatic muscles. Every actuator is supplied by one electronic servo valve in 3/3-way function. Part of this work is the derivation of the model description, which describes a high nonlinear dynamic behavior of the robot. Main focus is the physical model for the pneumatic muscle and a detailed model description for the servo valves. The aim is to control the tool center point (TCP) of the manipulator, which bases here on a fast subsidiary torque regulator of the drive system compensating the nonlinear effects. As the robot represents a MIMO system, a second control objective is defined, which corresponds here to the average pressure of each muscle-pair. An optimisation-strategy is presented to meet the maximum stiffness of the controlled drive system. As the torque controller assures a fast linear input/output behavior, a standardized controller is implemented which bases here on the Computed Torque Method to track the TCP. Measurement results show the efficiency of the presented cascaded control concept.

I. INTRODUCTION

Most robotic manipulators today apply electric drives in the form of servomotors or stepper motors. Hydraulic-drive robots are used for high-speed operations, but their main drawback lies in the lack of cleanliness. Using servopneumatic devices as actuator for robotics is up to now not state of the art although they are low in price and clean in their usage. One of the reason for that is their excessive nonlinear behavior [1], [2], [3]. Thereby the nonlinearity is caused by the flow characteristic of the servo-valve, by the gas compressibility, and in the presented work by the actuator. The set-up consists in this paper of a two-axis planar articulated robot serving by four pneumatic muscles. The main advantages of artificial muscles are: high power/weight ratio, usability in rough environments, and they are maintenance free. A major drawback of fluidic muscles is that they are just pulling actuators and possess a nonlinear contraction-pressure dependency of the force. Each muscle is served by one electronic proportional directional control valve in 3/3-way function.

The first part of this work deals with the physical model of the robot. The description of the fluid dynamic includes a detailed model of the servo-valve and the pressure behavior inside the muscles [4], [5]. Although several works are published about the nonlinear control

of pneumatic muscles, their force behavior was modelled as a rough nonlinear approximation by neglecting the energy, which is needed to deform the membrane [6], [7], [8], [9], [10], [11], [12]. In these approaches the force is always proportional to the pressure inside the muscle. That means the maximum contraction is mapped by one equilibrium point and is thereby pressure-independent. This paper presents measurement results (combined with those archived by using the finite-element-method), which shows that this approximation causes high failures as there exists a pressure-contraction depended equilibrium-line. Based on these characteristic, a new analytical approach is suggested resulting with a precise mapping of the muscle-force.

The control objective is to ensure a fast torque regulation of each joint in order to use for the position tracking standard control applications like computed-torque or PD-gravity controller [13]. A force controller, which bases on the feedback linearization, was successfully tested on an experimental setup consisting of one pneumatic muscle as actuator [11]. On the contrary to that, the presented robot is driven by four fluidic muscles yielding to a MIMO-system. That makes it possible to define a second control variable, which is in the presented case the average pressure inside the antagonist- and agonist-muscle. An optimization strategy is derived to define this mean pressure in such a way that a maximum stiffness of each joint is guaranteed.

II. SYSTEM ILLUSTRATION

The two-axis planar articulated robot (figure 1) is driven by 4 pneumatic muscles. This kind of actuator was presented in 1999 by the pneumatic manufacturer Festo [16]. It consists of a cylindrical, an isotropic flexible rubber tube and two connection flanges. When the muscle is inflated with compressed air, it widens. Hence a tension force, as well as a contraction movement in the longitudinal direction is created. The muscle is simply a flexible pulling actuator and cannot transmit pressure forces. The tension force is at its maximum at the beginning of the contraction and drops with the stroke to zero. It produces a maximum pulling force of 1800N, contracts up to 25% of its rated length and it possesses a very long life period of at least 10 million switching cycles. In the mapped adjustment, each joint can be moved around ± 15 degree. In order to achieve a larger sphere of action, it is possible to align the kinematics

(by varying the effective arm length or distance of the muscles to the axis). To inflate and deflate the muscles, four electronic proportional directional control valves in 3/3-way function are used. Two optical angle incremental encoders measure the position of each axis. Four pressure sensors gauge the pressure inside the tubes.

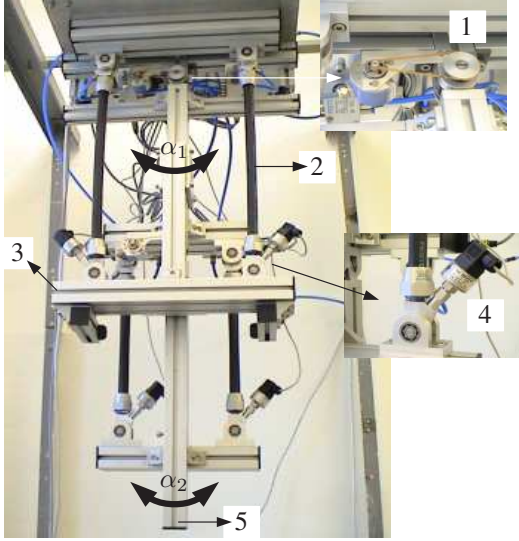


Fig. 1. Experimental setup; α_1 : joint angle of the first axis, α_2 : joint angle of the second axis, 1: angle encoder, 2: pneumatic muscle, 3: first axis, 4: pressure sensor, 5: second axis.

III. SYSTEM MODEL

To depict the dynamic and static behavior of the system, a mathematical set of nonlinear equations is derived. The initial point is to describe the pressure inside the muscle in relation to the valves air flow rate \dot{m}_i . The ideal gas equation describes the dependency of the gas mass: $m = \frac{pV}{RT}$, where m = gas mass inside the muscle, p = pressure inside the muscle, V = muscles inner volume, R = specific gas constant, T = gas temperature. Because the muscle tube consists of an elastomer, it can only pass partly the heat through the material. Any variation of the muscle's volume or pressure behave between the ideal condition isothermal and adiabatic and can be described by the polytrophic gas law: $p_b V_b^\chi = p_e V_e^\chi = \text{constant}$, where the index "b" indicates the beginning and index "e" points the end of the variation of the muscle's volume or pressure. The polytrophic exponent χ is identified to $\chi = 1.26$. The total differential of the latter mentioned combined with the ideal gas equation form the differential derivative for the pressure inside of each muscle "i":

$$\dot{p}_i = \frac{\chi}{V_i} \left(RT\dot{m}_i - p_i \dot{V}_i \right). \quad i = 1, \dots, 4 \quad (1)$$

The expression inside the brackets of equation (1) considers the power balance of the pressurized flow rate. The reciprocal volume before the bracket takes account of the

compressibility of the gas. The valves slide-stroke is controlled by an underlying position controller. That guarantees proportionality between the stroke position x_V and the set point voltage u . To achieve a high control frequency, the valve stroke is badly sealed in order to minimize static friction effects. That means, that the mass flow rate \dot{m}_i depends on an active flow rate \dot{m}_{12i} and a leakage flow rate \dot{m}_{23i} : $\dot{m}_i = \dot{m}_{12i} - \dot{m}_{23i}$, $i = 1, \dots, 4$. [5] and [4] suggest to describe those effect with an equivalent network, which is build up by two air resistances $C_{12}(x_V)$ and $C_{23}(x_V)$ depending respectively on the valve stroke x_V . The leakage and active mass flow rate are expressed by the common pneumatic flow rate equation [17]:

$$\begin{aligned} \dot{m}_i &= C_{12i}(x_{Vi})\rho_0 p_s \Psi \left(\frac{p_i}{p_s}, b_{12i}(x_{Vi}) \right) \dots \quad i = 1, \dots, 4 \\ &\dots - C_{23i}(x_{Vi})\rho_0 p_i \Psi \left(\frac{p_0}{p_i}, b_{23i}(x_{Vi}) \right). \end{aligned} \quad (2)$$

where p_s = supply pressure, p_0 = atmospheric pressure, p_i = pressure inside each muscle, and ρ_0 = atmospheric air density. The function Ψ considers the state of the flow rate. In the case the pressure ratio at an air resistance is smaller than the critical pressure ratio b , the flow rate is limited by the sonic speed, which results that Ψ equalling one. Is the pressure ratio higher than the critical one, the flow function Ψ is proportional to the square root of the pressure ratio:

$$\Psi \left(\frac{p_{sec}}{p_{prim}}, b \right) = \begin{cases} 1, & \frac{p_{sec}}{p_{prim}} < b, \\ \sqrt{1 - \left(\frac{\frac{p_{sec}}{p_{prim}} - b}{1 - b} \right)^2}, & \frac{p_{sec}}{p_{prim}} \geq b, \end{cases} \quad (3)$$

where p_{prim} = pressure in front, and p_{sec} = behind the considered air resistance. As mentioned in [5], the critical pressure ratio b depends also on the valve-slide stroke position. The air conductivities C_{12} , C_{23} and the critical pressure ratios b_{12} , b_{23} are identified experimentally. The dynamic response of the servo valve is equivalent to a frequency of approximately $100Hz$, for a desired control frequency of about $20Hz$ this effect is negligible. As in [5] already shown, the air conductivity and the critical pressure ratio depends strongly on the input voltage of the valve. Edges inside the valve cause turbulent flow effects especially at high flow rates. In this case the air resistance rises, while the flow rate behaves earlier in the subcritical state as ideally supposed. This property shows figure 2 and figure 3: at high input voltages, the air conductivities flattens and the critical pressures falls up to $b = 0.32$. In the range of zero volt, one can see that the conductivities brake down significantly. This effect is provoked by the covering of the upper and lower steering edge of the valve stroke in order to guarantee just small air leakage around $u = 0V$.

Next, it is necessary to describe the inner volume of the muscles, as it characterizes the dynamic pressure build-up inside the bladder (eq. (1)). It is proofed by measurements, that the inner volume of the muscle depends merely on the contraction length and not on the pressure. As already discussed in [11], the volume is experimentally identified and approximated by a polynomial function of third order depending on the contraction z_i :

$$V_i(z_i) = \sum_{j=0}^3 c_j z_i^j. \quad i = 1, \dots, 4 \quad (4)$$

The physical model of the muscle force behavior is derived for example by [15], [8], [10], [11]. The primary idea of that is the energy conservation of mechanical and gas energy displacements. The approaches results thereby always to a muscle force behavior, which is proportional to the pressure: $F_m = p \cdot \frac{dV}{dz}$. That means, elasticity effects of the tensile material are fully neglected. In order to achieve high control frequencies of the closed loop scheme, an exact mapping of the force behavior is essential. In the following an analytical muscle-force function is presented, which matches the measured one at least to $\pm 15N$. Thereby the pneumatic muscle is considered as an one way cylinder (with virtual flexible diameter as a function of the contraction), which moves against a spring (with a contraction depended spring tension). The function of the muscle force F_m can be described as:

$$F_m(p, z) = p \cdot A(z) - F(z) \quad (5)$$

where $A(z) =$ virtual piston area and $F(z) =$ the tension force of the spring, depending both on the contraction z , and $p =$ absolute pressure inside the muscle. The virtual piston area is in this approach supposed to be a polynomial function of the second order. To map the strong rise of the force at small contraction displacements (see figure 4) precisely, it would be necessary to use a polynomial function of the 30th order for the spring force-behavior. To reduce the order, a polynomial of the 3rd order is supposed, which is added by a power function. Hence, the analytical muscle force function yields to:

$$F_m(p, z) = p \cdot \sum_{j=0}^2 d_j z^j - \left(\sum_{j=0}^3 e_j z^j + e_4 z^{2/3} \right). \quad (6)$$

The parameters d_j, e_j, e_4 are identified by using optimization algorithms to minimize the mean square-failure between analytical and numerical force characteristics. The result is shown in figure 5. One can see failures of approximately $\pm 5N$ inside the characteristic diagram and failures up to $\pm 15N$ at the outer line. Function (6) is used to calculate the torque applied on the axis of the robot. The driving torque T_1, T_2 on the first and second joint is given by:

$$\begin{aligned} T_1 &= F_{m1}(\alpha_1, p_1) \cdot s_1(\alpha_1) - F_{m2}(\alpha_1, p_2) \cdot s_2(\alpha_1), \\ T_2 &= F_{m3}(\alpha_2, p_3) \cdot s_3(\alpha_2) - F_{m4}(\alpha_2, p_4) \cdot s_4(\alpha_2), \end{aligned} \quad (7)$$

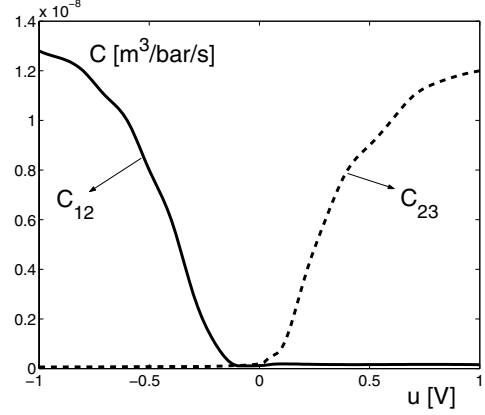


Fig. 2. Identified air conductivity in respect of the input voltage of the valve.

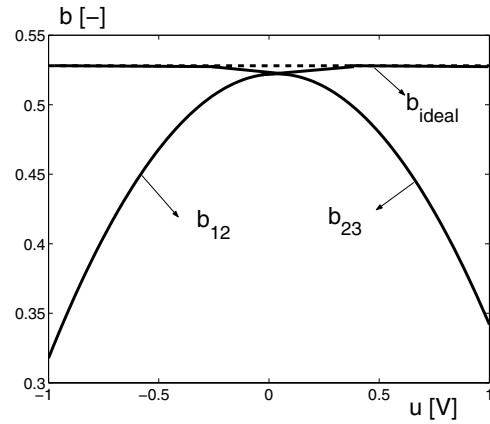


Fig. 3. Identified critical pressure ratio in respect of the input voltage of the valve.

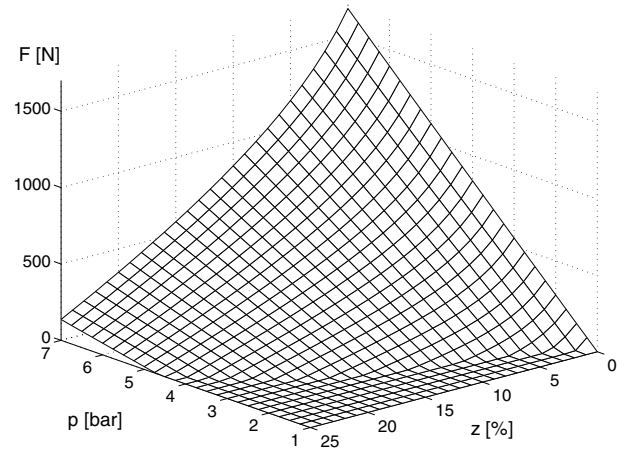


Fig. 4. Measured force characteristic of the pneumatic muscle MAS-20 (Festo).

thereby the contraction z of the force eq. (6) is expressed by the joint angles α_i , which are expressed by trigonometrical transformation based on the geometry of the robot, $s_i =$ the effective lever arm depending on the joint angles, and

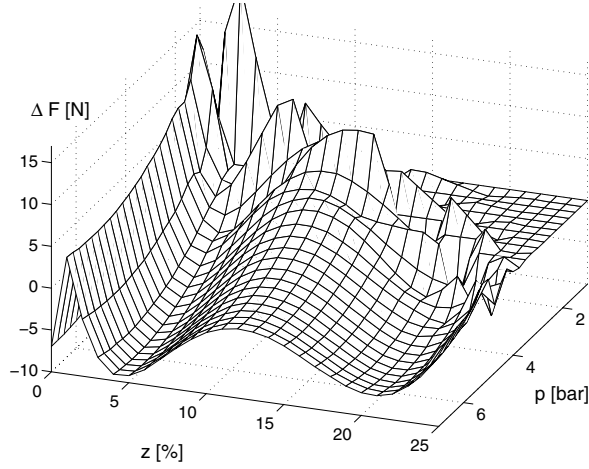


Fig. 5. Error in force of the analytical muscle-force function.

p_i is the pressure inside each muscle. Using the Lagrange formalism to derive the dynamic model of the motion yields to:

$$\underline{M}(\underline{\alpha})\ddot{\underline{\alpha}} + \underline{C}(\underline{\alpha}, \dot{\underline{\alpha}}) + \underline{G}(\underline{\alpha}) = \underline{T}(\underline{\alpha}, \underline{p}), \quad (8)$$

where \underline{M} = mass matrix, \underline{C} = matrix of coriolis and centripetal effects, \underline{G} = gravity matrix, $\underline{\alpha}$ = vector of the joint angle, \underline{p} = vector of the applied pressure, and \underline{T} = the torque matrix given by eq. (7). As the joint is hinged nearly frictionless, those effects are neglected.

IV. CONTROLLER DESIGN

The ambition is to track the tool center point (TCP) of the robot. In this work it is developed a cascaded control structure. The outer control loop consists of the "Computed-Torque Method", which is state of the art [13]. Thereby the dynamic coupling of the motion is fully compensated. The input signals are the reference trajectory of each joint, the output of the outer control is thereby the reference torque, which has to be applied by the inner control using an accurate and fast torque regulator. As the system has MIMO, it is chosen the mean pressure of antagonist- and agonist-muscle, which can be interpreted as a second control variable. The whole structure demonstrates figure 6.

A. Outer control loop: Trajectory tracking

As the dynamic model (8) is differential flat, it can be easily computed a feedforward control:

$$\underline{T}_{ref} = \underline{M}(\underline{\alpha}_{ref})\ddot{\underline{\alpha}}_{ref} + \underline{C}(\underline{\alpha}_{ref}, \dot{\underline{\alpha}}_{ref}) + \underline{G}(\underline{\alpha}_{ref}). \quad (9)$$

The reference position $\underline{\alpha}_{ref}$ and its derivatives denote the desired trajectory, which are calculated by a path planner. Next, the acceleration vector of eq. (9) is set to a new input $\underline{\nu} =: \ddot{\underline{\alpha}}$ and the reference variables are exchanged by the measured one. In order to guarantee a fast and stable

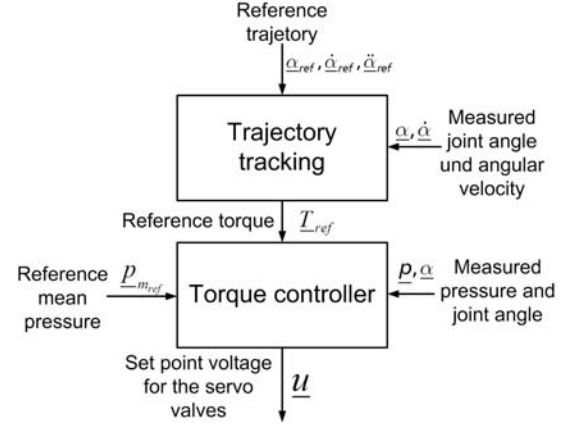


Fig. 6. Structure of the cascaded control concept.

tracking, the new input is calculated by a feedforward and feedback control:

$$\underline{\nu} = \ddot{\underline{\alpha}}_{ref} + \underline{K}_1(\dot{\underline{\alpha}} - \dot{\underline{\alpha}}_{ref}) + \underline{K}_0(\underline{\alpha} - \underline{\alpha}_{ref}). \quad (10)$$

Thereby the matrix \underline{K}_1 and \underline{K}_0 are the control gains for the angular velocity and angle error respectively, and are chosen by pole assignment. Combining eq. (10) with eq. (9) leads to the trajectory tracking law:

$$\underline{T}_{ref} = \underline{M}(\underline{\alpha})\underline{\nu} + \underline{C}(\underline{\alpha}, \dot{\underline{\alpha}}) + \underline{G}(\underline{\alpha}). \quad (11)$$

B. Inner control loop: Torque regulator

The main object of the inner control loop is to track the reference torque, which is computed by the latter presented superior trajectory control. As the torque of each joint depends not on the absolute pressure inside the muscles, eq. (7) defines an overdetermined set of equations by solving the pressures p_i . Therefore an additional control variable is suggested, which is in this paper the pressure-average of each muscle-pair:

$$\begin{aligned} p_{m1ref} &= (p_{1ref} + p_{2ref})/2, \\ p_{m2ref} &= (p_{3ref} + p_{4ref})/2, \end{aligned} \quad (12)$$

where $p_{mi_{ref}}$ = reference mean pressure of antagonist- and agonist-muscle in respect of the reference pressure of each muscle $p_{i_{ref}}$. Combining eq. (7) with eq. (12) (thereby the variables T_1, T_2 and p_i of eq. (7) are replaced by the referenced one), it is possible to derive the four reference pressures $p_{i_{ref}}$ in respect of a demanded reference torque \underline{T}_{ref} and a freely chosen average pressure p_{m1ref}, p_{m2ref} of the two muscles pairs:

$$\underline{p}_{ref} = \underline{\Theta}^{-1}(\underline{p}_{m_{ref}}, \underline{T}_{ref}, \underline{\alpha}), \quad (13)$$

where $\underline{\Theta}^{-1}$ is the inverse function of eq. (7), combined with eq. (12). To stabilize the pressure inside the muscles, a nonlinear controller is used, which bases on the exact input-output linearizing method [14]. Thereby the flow eq. (1) is added by the mass flow rate eq.(2), the volume function (4) is expressed by the joint angles, and the slide-stroke

of the valve is supposed to be proportional to the input. By converting this differential equation to the valves input voltages, the inverse mapping of the pressure behavior is achieved by:

$$\begin{aligned} \dot{m}_{i_{ref}} &= \frac{1}{RT} \left(\frac{V_i(\alpha_1, \alpha_2)}{\chi} \dot{p}_i + \dot{V}_i(\alpha_1, \alpha_2) p_i \right), (14) \\ u_i &= \vartheta_i^{-1}(\dot{m}_{i_{ref}}, p_i, \epsilon), \quad i = 1, \dots, 4 \end{aligned} \quad (15)$$

where ϑ^{-1} indicates the numerically inverted valve function (2), and ϵ indicates the constant gain to express the valve voltage in respect of the valve stroke $u_i = \epsilon x_{iV}$. As the pressure derivation is not part of the system, it can be chosen freely:

$$\nu_i \stackrel{!}{=} \dot{p}_i, \quad i = 1, \dots, 4 \quad (16)$$

where ν denotes the external reference input. To stabilize the pressure, the external reference input is chosen so as to assure a vanishing tracking error $e_i = p_{i_{ref}} - p_i$:

$$\nu_i = \dot{p}_{i_{ref}} + K_i(p_{i_{ref}} - p_i), \quad i = 1, \dots, 4 \quad (17)$$

where $K_i > 0$ specifies the control frequency and $p_{i_{ref}}$ denotes the desired pressure inside each muscle represented by eq. (13). The resulting structure of the torque regulator can be seen in figure 7. While the reference torque is set

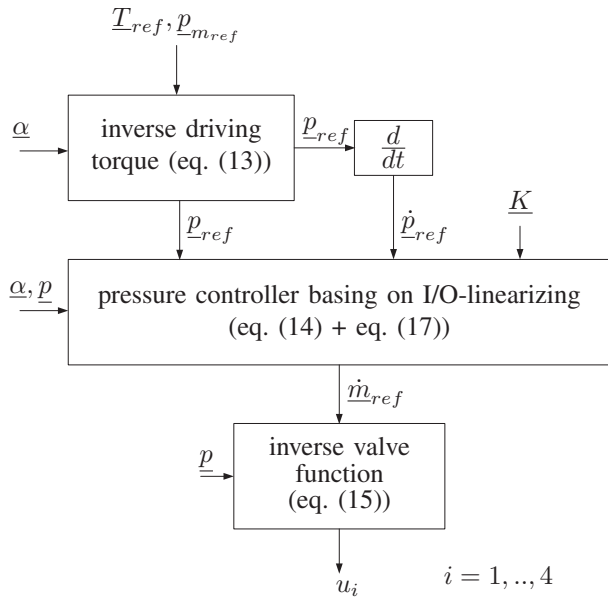


Fig. 7. Structure of the torque regulator.

by the superior trajectory controller, the reference average pressure $p_{m_{ref}}$ can be chosen in a wide range. Thereby it characterizes the stiffness of each joint. In the following an optimization strategy is introduced, which guarantees a maximum stiffness. This is achieved by maximizing the amplification of the plant controlled system, which means, that a variation of the reference torque produces just a minimum signal in u_i . Assuming a linear air conductivity of the valve, negligible air leakage and a constant critical

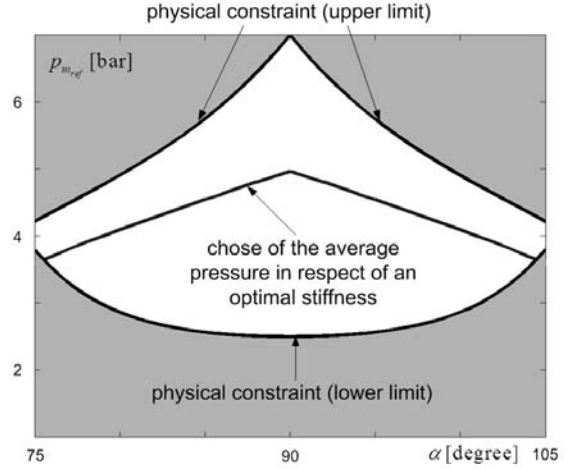


Fig. 8. Computation of the optimal average pressure in order to maximize the stiffness.

pressure ratio b , the differential equation of the pressure eq. (1) and eq. (2) can be written as:

$$\begin{aligned} \dot{p}_i &= \frac{\chi}{V_i} \left(RT \psi_i(p_i) \cdot u_i - p_i \dot{V}_i \right), \quad i = 1, 3. \quad (18) \\ \dot{p}_{i+1} &= \frac{\chi}{V_{i+1}} \left(RT \psi_{i+1}(p_{i+1}) \cdot u_{i+1} - p_{i+1} \dot{V}_{i+1} \right), \end{aligned}$$

where the index "i" and "i+1" label the antagonist- and agonist-muscle of each joint, $\psi(p)$ denotes the air flow characteristic given by eq. (3) and eq. (2). The amplification of the pressure plant has the form $\frac{\chi}{V} (RT \psi(p))$. Assuming, that no external torque is applied, p_i and p_{i+1} can be expressed by the references average pressure using eq. (13). By setting the average pressure at a high level, it can be fast inflated but slowly deflated, if a low average pressure is used, this results to a slow inflating but fast deflating. To find the optimal average pressure, it is given the summation of the pressure-amplification:

$$\begin{aligned} Q_1 &= \frac{\psi_1(p_{1m_{ref}}, \alpha_1)}{V_1(\alpha_1)} + \frac{\psi_2(p_{1m_{ref}}, \alpha_1)}{V_2(\alpha_1)} \rightarrow \max, \\ Q_2 &= \frac{\psi_3(p_{2m_{ref}}, \alpha_2)}{V_3(\alpha_2)} + \frac{\psi_4(p_{2m_{ref}}, \alpha_2)}{V_4(\alpha_2)} \rightarrow \max, \end{aligned} \quad (19)$$

which has to be maximized in respect of the average pressure $p_{1m_{ref}}$ and $p_{2m_{ref}}$. In consideration of the maximization of the allowed working range (which is restricted by the geometry and the pressure limitation) and the avoidance of any discontinuities, the result is shown in figure 8 just for the upper axis.

V. EXPERIMENTAL RESULTS

The control frequency of the trajectory controller is chosen to 7Hz, and the control frequency of the presented torque regulator is set to 20Hz. Figure 9 shows the joint angle after a stepwise disturbance. One can see a good damping behavior. Figure 10 and 11 indicate the reference and measured angle of a coupled tracking movement.

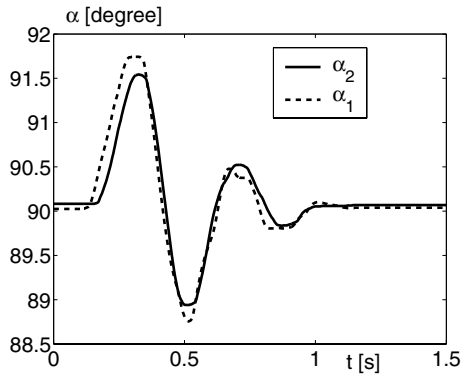


Fig. 9. Joint angles after a stepwise disturbance.

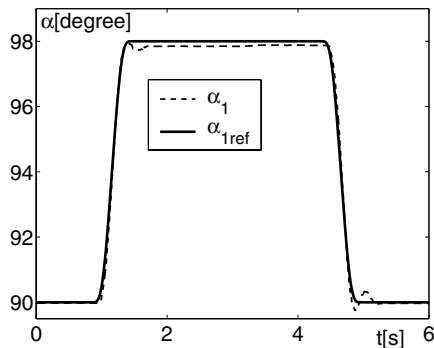


Fig. 10. Reference and measured joint angle α_1 (coupled motion illustrated in fig. 11)

VI. CONCLUSION

This paper presents a physical model based torque regulator for a two-axis planar articulated robot, which is driven by four pneumatic muscles. It is derived a detailed model of the dynamic pressure behavior inside the muscles, including the modelling of the servo-valve. The used fluidic muscle comes with a high nonlinearity of the force. It is presented a new analytical approach to map the static contraction-pressure dependency of the muscle-force. The motivation of the controller is to ensure a fast torque regulation of each joint in order to use standard tracking control application, which bases for example on the Computed-Torque method. This means the driving torque has to equal the desired one. To achieve this, the paper derives a control strategy, which compensates the nonlinear effects of the pressure dynamic and the nonlinear torque characteristic of the actuators. As the robot is a MIMO system, it is possible to chose a further control variable, which corresponds in this approach to the average pressure of each muscle-pair. In the sense of an optimization strategy, the average pressure is chosen in such a way to ensure a maximum stiffness of the drive system.

REFERENCES

[1] F. Takemura, S.R. Pandian, S. Kawamura, Y. Hayakawa, "Observer design for control of pneumatic cylinder actuators," in *PTMC 99, Bath Workshop on Power Transmission and Motion Control*, Bath, Sep 8.-10.9.1999, pp. 223-236, 1999.

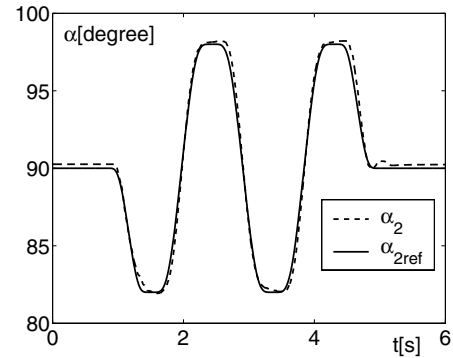


Fig. 11. Reference and measured joint angle α_2 (coupled motion illustrated in fig. 10)

- [2] O. Sawodny, A. Hildebrandt, "Aspects of the control of differential pneumatic cylinders", in *10th Japanese-German Seminar on Nonlinear Problems in Dynamical Systems*, Kanazawa, pp 247-256, 2002.
- [3] G. Tao, P.V. Kokotovic, "Adaptive control of systems with actuator and sensor nonlinearities", in *John Wiley & Sons, INC., New York*, 1996.
- [4] X. Brun, M. Belgharbi, S. Sesmat, D. Thomasset, S. Scavarda "Control of an electropneumatic actuator, comparison between some linear and nonlinear control laws." in *Journal of Systems and Control Engineering* 213, pp 387-406, 1999.
- [5] M. Göttert, "Bahnregelung servopneumatischer Antriebe", Shaker Verlag, 2004.
- [6] D. W. Repperger, K. R. Johnson, C. A. Philips, "Nonlinear feedback controller design of a pneumatic muscle actuator system," in *Proc. 1999 American Control Conference*, San Diego, pp. 1525-1529, 1999.
- [7] R. Q. van der Linde, "Design, analysis, and control of a low power joint for walking robots, by phasic activation of McKibben muscles," in *Proc. IEEE Transactions on Robotics and Automation*, Vol. 15, No. 4, pp. 599-604, 1999.
- [8] No-Cheol Park, Hyun-Wug Park, Hyun-Seok Yang, and Young-Pil Park "Position and force control of 2 D.O.F. flexible manipulator with artificial pneumatic muscle actuators", in *Journal Of Vibration And Control*, Vol.40, pp. 239-253, 2002.
- [9] A. Hildebrandt, O. Sawodny, R. Neumann, A. Hartmann, "A flatness based design for tracking control of pneumatic muscle actuator", *Seventh International Conference on Control, Automation, Robotics & Vision*, Singapore, pp 1156-1161, 2002.
- [10] N. Yee, G. Coghill "Modelling of a novel rotary pneumatic muscle" in *Proc. Australian Conference on Robotics and Automation*, Auckland, pp. 186-190, 2002.
- [11] A. Hildebrandt, O. Sawodny, R. Neumann, A. Hartmann, "A cascaded tracking control concept for pneumatic muscle actuators", *European Control Conference 2003 (ECC03)*, Cambridge UK, (CD-Rom), 2003.
- [12] R. Van Ham, F. Daerden, B. Verrelst, & D. Lefeber "Control of a joint actuated by two pneumatic artificial muscles with fast switching on-off valves" in *6th National congress on theoretical and applied mechanics*, Ghent, May 2003, paper no. 075 (CD-ROM), 2003.
- [13] R.J. Schilling, "Fundamentals of robotics, analysis & control", Prentice Hall, 1990.
- [14] A. Isidori, "Nonlinear control systems," Springer Verlag, 3rd edition, 1995.
- [15] C. P. Chou, B. Hannaford, "Measurement and modeling of McKibben pneumatic artificial muscle," in *Proc. IEEE Transactions on Robotics and Automation*, Vol. 12, No. 1, pp. 90-102, 1996.
- [16] R. Neumann, M. Goettert, "Roboter mit servopneumatischen Antrieben," in *Proc. 4. Deutsch-Polnisches Seminar "Innovation und Fortschritt in der Fluidtechnik"*, Sopot, pp. 205-223, 2001.
- [17] W. Backe, O. Ohlgschlager, "A model of heat transfer in pneumatic chambers," in *Journal of Fluid Control*, Vol. 20, No. 1, pp. 67-78, 1989.